Domain engineered states over various length scales in (001)-oriented Pb (Mg 1/3 Nb 2/3) O 3 - x % Pb Ti O 3 crystals: Electrical history dependence of hierarchal domains

Feiming Bai, Jiefang Li, and D. Viehland

Citation: Journal of Applied Physics **97**, 054103 (2005); doi: 10.1063/1.1855392
View online: http://dx.doi.org/10.1063/1.1855392
View Table of Contents: http://scitation.aip.org/content/aip/journal/jap/97/5?ver=pdfcov
Published by the AIP Publishing

Domain engineered states over various length scales in (001)-oriented $Pb(Mg_{1/3}Nb_{2/3})O_3$-x%$PbTiO_3$ crystals: Electrical history dependence of hierarchal domains

Feiming Bai, Jiefang Li, and D. Viehland
Department of Materials Science and Engineering, Virginia Tech, Blacksburg, Virginia 24061

(Received 26 August 2004; accepted 10 December 2004; published online 11 February 2005)

The dependence of the domain structure on poling for (001)-oriented $Pb(Mg_{1/3}Nb_{2/3})O_3$-x%$PbTiO_3$ crystals with $x=20$, 30, 35, and 40 has been investigated by scanning force microscopy in the piezoresponse mode and by polarized optical microscopy. The results demonstrate a domain hierarchy on various length scales, ranging from nanometers to millimeters, which is notably dependent upon the electrical history of the specimen. The results provide important insights into the nature of the domain engineered state in these crystals. © *2005 American Institute of Physics*. [DOI: 10.1063/1.1855392]

I. INTRODUCTION

Single crystals of $Pb(Mg_{1/3}Nb_{2/3})O_3$-x%$PbTiO_3$ (PMN-x%PT) and $Pb(Zn_{1/3}Nb_{2/3})O_3$-x%$PbTiO_3$ (PZN-x%PT) have attracted much attention as high performance piezoelectric actuator and transducer materials. A *domain-engineered state*, due to an electric field induced rhombohedral-to-tetragonal phase transition, was first proposed by Park and Shrout[1] to explain the ultrahigh electromechanical properties. Structural studies of the similar system $Pb(Zr_{1-x}Ti_x)O_3$ (PZT) have since revealed the existence of new ferroelectric monoclinic (M) phases, sandwiched between the rhombohedral (R) and tetragonal (T) ones, near a morphotropic phase boundary (MPB).[2–4]

The crystalline solution PMN-x%PT is known to have complex structure-property relationships. In the annealed or zero-field-cooled (ZFC) condition for $x<35$, a relaxor ferroelectric state exists, which is characterized by a frequency dispersive dielectric maximum.[5,6] Phase transformation investigations by x-ray diffraction (XRD) and neutron scattering have shown a T phase for $x>35$, a monoclinic M_C phase for $30<x<35$, a R phase for $25\approx x<30$,[7,8] and a slightly distorted pseudocubic phase designated as X for $x<25$.[9,10] Corresponding to these structural studies, counterpart investigations of the domain structure evolution with increase of PT concentration have also been performed by polarized optical microscopy (POM),[11–13] and by transmission electron microscopy (TEM).[14,15] For example, spindlelike rombohedral domains, monoclinic domains with various optical extinction angles, and stripelike tetragonal domains have been reported in PMN-24%PT,[11] PMN-33%PT,[12] and PMN-50%PT crystals,[13] respectively. In addition, previous TEM studies[14,15] have revealed miniature polar nanodomains (PND) of several hundred angstroms in size for $x<30$, where the average size decreased with decreasing x; small cross-hatched tweedlike domains for $30\approx x<35$; and normal micronsized 90° domains in the T phase.

In the poled or field-cooled (FC) condition, the structure-property relationships of PMN-x%PT are known to be significantly different, relative to that of the ZFC. For example, the relaxor state of the ZFC condition is altered into a normal ferroelectric one in the FC condition that has a diffuse transformation and remanence.[16–18] Structural investigations of the FC by x-ray and neutron scatterings have showed that the stable structure is the T phase for $x>35$, the monoclinic M_C phase for $30<x<35$, and the monoclinic M_A phase for $20\approx x<30$ at 300 K.[19,20] In the ZFC condition at a constant temperature of 300 K, an irreversible $R\rightarrow M_A$ transition has been reported with increasing E for $x=30$;[20] whereas, the stable structure remains M_C with increasing E for $x=35$. Corresponding investigations by POM have revealed micronsized domains[18] in the FC, whereas images obtained from the same crystal in the ZFC are featureless.

However, systematic investigations have not yet been performed comparing the morphological details over a range of length scales for the ZFC and FC domain structures, which maybe important to understand the nature of the domain-engineered state and resultant anomalous electromechanical properties. The lack of such prior studies may in part be due to (i) insufficient resolution of POM to reveal small scale features and (ii) difficulties in maintaining the fully poled condition upon ion milling a TEM specimen. In recent years, scanning force microscopy (SFM) in the piezoresponse mode has been used to study ferroelectric domains.[21,22] This technique is based on the detection of local vibrations of a ferroelectric sample induced by a testing ac signal applied between the conductive tip of the SFM and the bottom electrode of the sample. The oscillations of the sample underneath the tip modulate the global deflection signal and are detected using a lock-in technique.[23] Small irregular domain features have been reported in unpoled and poled PZN-x%PT and PMN-x%PT crystals,[24,25] demonstrating that small scale ferroelectric domain features can be identified by this method.

The purpose of this investigation was to determine the ZFC and FC domain structures of (001)-oriented PMN-x%PT crystals, for $20<x<40$, by piezo-response force microscopy (PFM). Investigations have focused on revealing (i) how the domain structure changes between phase R in the ZFC condition and phase M_A in the FC condition; (ii) how

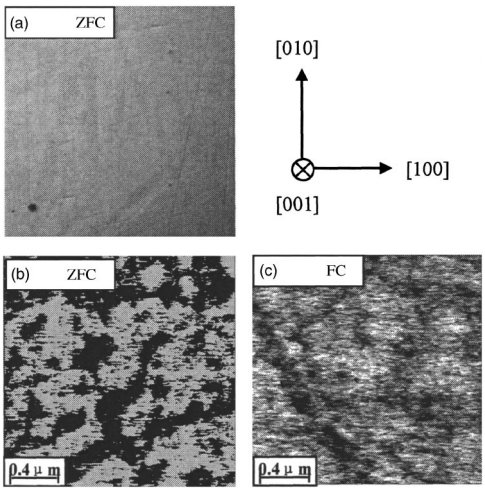

FIG. 1. Domain hierarchy of (001)-orientated PMN-20%PT in the ZFC and FC conditions. (a) Lack of macrodomain plates in the POM image for the ZFC condition, a similar image was found for the FC condition; (b) PFM image for the ZFC condition; and (c) PFM image for the FC condition.

the domain structure of phase M_C and phase T differ between ZFC and FC; and (iii) whether the domain structure of each depends on the range of length scales that are studied.

II. EXPERIMENTAL PROCEDURE AND SAMPLE PREPARATION

Single crystals of PMN-x%PT (x=20, 30, 35, and 40) were grown by a top-seeded modified Bridgman method.[26,27] The crystals obtained from HC Materials (Urbana, IL) were cut into plates with typical dimensions of $4\times4\times0.3$ mm^3, and were oriented along the (001) direction. The top faces of the crystals were polished to 0.25 μm finishes. SFM images were obtained in the piezoresponse mode using a commercial unit (Vecoo DI 3100a). All scans were performed at room temperature using a conductive silicon tip coated with cobalt (tip radius of ~20 nm). Gold electrodes were deposited on the bottom face of each sample by sputtering. The electroded faces were then glued to the SFM sample stage. An ac voltage with a frequency of 20 kHz and amplitude between 1 and 10 V was applied between the conductive tip and the bottom gold electrode. Scans were taken by rastering the SFM tip on the top faces (unelectroded side). Measurements were first performed on annealed crystals. Subsequently, investigations were performed on crystals that had been poled under a field of E=4 kV/cm.

III. RESULTS

A. PMN-20%PT

Figure 1 shows POM and PFM images taken over various length scales for (001) PMN-20%PT in the ZFC and FC (E=6 kV/cm) conditions. In the ZFC condition [see Fig. 1(a)], which is of the X phase,[4–6] no larger scale domain features were found by POM. Similar POM images were obtained for the FC condition, but are not shown. However, miniature polar domains of nanometer size (PND) were found in the PFM images, whose morphology and distribution were quite irregular, as shown in Fig. 1(b). The volume

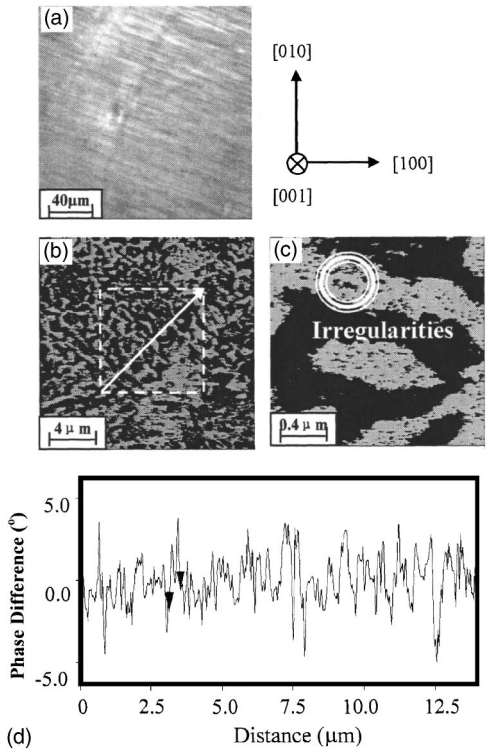

FIG. 2. Domain hierarchy of (001)-orientated PMN-30%PT in the ZFC condition, which is of the R phase. (a) Spindlelike macrodomains with [110] preferred orientation by POM; (b) wavelike self-assembled domains by PFM; (c) high resolution PFM image illustrating nonsmooth domain boundaries and irregularity; and (d) cross-sectional line analysis normal to [110].

fractions of light and dark color regions, representative of different domain variants, were roughly equal. In the FC condition [see Fig. 1(c)], miniature domains of irregular shape remained present, and there was no clear evidence of significant domain growth. However, the relative volume fraction of one domain variant was strongly favored over the others, indicating an alignment of PND along an easy axis.

B. PMN-30%PT

Figure 2 shows POM and PFM images taken over various lengths scales for (001) PMN-30%PT in the ZFC condition. The stable phase is of the R structure.[3,4] Figure 2(a) shows a POM image, which reveals the presence of macrodomain plates oriented along {110} that are ~1 μm in width and ~40 μm in length. Inside of the macroplates are "wavy" domains with an average length of ~1 μm that have some preferential orientation along {110}, as shown in the PFM image of Fig. 2(b). Figure 2(c) shows a higher resolution PFM image. This image illustrates (i) that the domain boundaries are notably nonsmooth; (ii) that there are irregularities of similar size and morphology to PND within the wavy domains; and (iii) that there is a lack of morphological regularity. Cross-sectional line analysis revealed an average domain spacing of ~0.25 μm, where the phase difference fluctuated notably as a function of the spatial coordinate along {110}.

Figure 3 shows POM and PFM images taken over various lengths scales for (001) PMN-30%PT in the FC condition. The stable phase is of the M_A structure.[19,20] Figure 3(a)

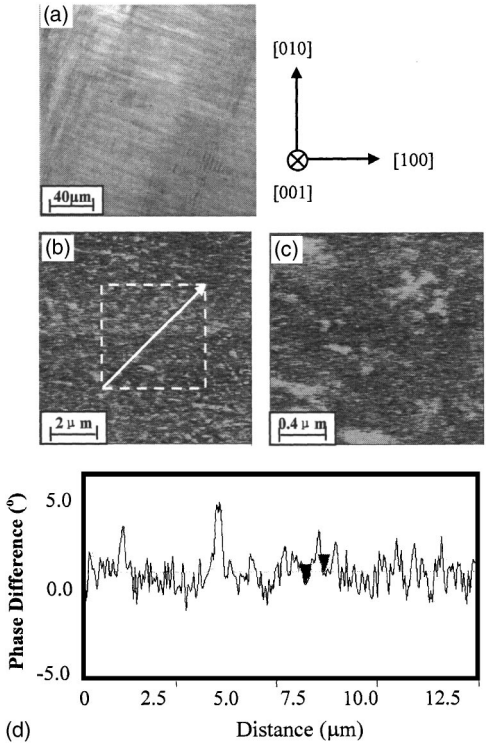

FIG. 3. Domain hierarchy of (001)-orientated PMN-30%PT in the FC condition, which is of the M_A phase. (a) Spindlelike macrodomains with ⟨110⟩ preferred orientation by POM; (b) identification of polar nanodomains or PND by PFM; (c) high resolution PFM image illustrating size of PND; and (d) cross-sectional line analysis normal to [110].

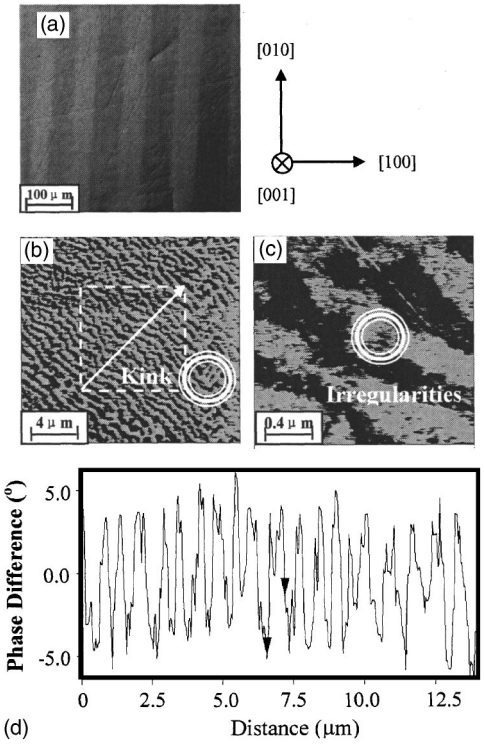

FIG. 4. Domain hierarchy of (001)-orientated PMN-35%PT in the ZFC condition, which is of the M_C phase. (a) Striplike macrodomains with [100] preferred orientation by POM; (b) domain striations with [110] preferred orientation by PFM, and kinks are illustrated at domain boundaries; (c) high resolution PFM image; and (d) cross-sectional line analysis normal to [110].

shows a POM image that reveals tiny domains developing inside spindlelike domains, forming at almost 90° angles. The spindle domains are ~1 μm in width and maintain a {110} orientation, consistent with the polarization of the M_A phase being confined to the $(1\bar{1}0)_c$ plane. The internal structure of the FC domains was probed using PFM, as shown in the image given in Fig. 3(b). Miniature polar domains were found in the PFM images, whose morphology and distribution were quite irregular. Figure 3(c) shows a higher resolution PFM image. Comparisons of Figs. 2(c) and 3(c) in the ZFC and FC conditions will reveal a dramatic decrease in the size of the miniature domains on poling for PMN-30%PT. In the ZFC condition, the miniature domains demonstrate a significant degree of self-assembly, although irregularities of similar size and morphology to PND were found within the domain striations; whereas in the FC condition, self-assembly was no longer apparent on a length scale distinguishable by PFM, rather only the irregularities were apparent. Cross-sectional analysis confirmed a significant decrease in the size of the miniature domains in the FC condition (0.04 μm), relative to that of the ZFC (0.25 μm in width and microns in length).

C. PMN-35%PT

Figure 4 illustrates the domain structure characterization results taken over various length scales for (001)-oriented PMN-35%PT in the ZFC condition. The stable phase is of the M_C structure.[3,4] Figure 4(a) shows a POM image, which reveals the presence of macrodomain plates oriented along {001} that are ~50 μm wide. Inside the macroplates are alternating domain striations oriented along {110}, as shown in the PFM image of Fig. 4(b). Kinks in the domain striations were found, as illustrated by the circled area in the figure. The kinks are 90° twins between {110} striations, with their twin walls along {001}. Figure 4(c) shows a higher resolution PFM image. Under higher resolution, the domain striations were found to be notably rough and nonuniform in thickness. Again, irregularities of similar size and morphology to PND were found within the domain striations. A cross-sectional line analysis taken along the {110} plane is shown in Fig. 4(d), illustrated by the white arrow. The average domain spacing was ~0.35 μm, where the spacing and phase contrast between neighboring variants varied notably. In addition, cross-sectional analysis indicated pronounced contrast variation within a domain, as illustrated between the two triangles in the figure.

Figure 5 shows POM and PFM images taken over various lengths scales for (001) PMN-35%PT in the FC condition. The stable phase is also of the M_C structure.[19,20] Figure 5(a) shows a POM image that reveals the presence of macrodomain plates oriented along {001} that are ~50 μm wide, which is quite similar with the POM image in ZFC condition. The internal structure of the FC macrodomains was probed using PFM, as shown in the image given in Fig. 5(b). Figure 5(c) shows a higher resolution PFM image. Inside the macroplates was found alternating domain striations; however, comparisons of the higher resolution PFM images in the ZFC and FC conditions, Figs. 4(c) and 5(c), will clearly reveal two important differences. First, the FC domain stria-

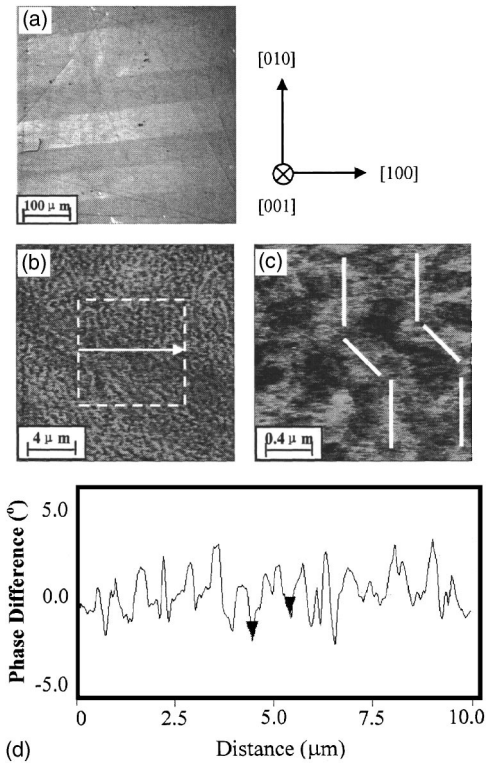

FIG. 5. Domain hierarchy of (001)-orientated PMN-35%PT in the FC condition, which is of the M_C phase. (a) Stripelike macrodomains with [100] preferred orientation by POM; (b) domain striations with either [110] or [010] preferred orientation by PFM, which are of notably smaller length than those of the ZFC condition; (c) high resolution PFM image; and (d) cross-sectional line analysis parallel to [100].

tions were notably shorter in length than the corresponding ZFC ones—less than 1 μm compared to tens of microns, although the widths were quite similar. Second, the FC domain striations were zigzagged between {010} variants about the {110}, as indicated in Fig. 5(c). In both the FC and ZFC conditions, internal irregularities of similar size to PND were found. Cross-sectional analysis yielded similar average domain sizes for both the FC and ZFC conditions ($\sim$0.25 μm).

D. PMN-40%PT

Figure 6 shows POM and PFM images taken over various lengths scales for (001)PMN-40%PT in the ZFC condition, which is of the *T* phase.[3,4] Macrodomain plates oriented along {001} are apparent in the POM image of Fig. 6(a). The plates are similar to those of PMN-35%PT, except for (i) a fibrous internal structure within the plates is also oriented along {001} and (ii) 90° fringes indicative of larger transformation strains. The internal structure of the macrodomain plates was identified to be alternating (001)-oriented lamella domains that were broken in the longitudinal direction, as shown in the PFM image of Fig. 6(b). Figure 6(c) showed the high resolution PFM image of the broken lamella domains. Again, irregularities of about the same size as PND were found to exist within the lamella. Cross-sectional analysis, taken along the {001} plane, is shown in Fig. 6(d). The average domain spacing was $\sim$2 μm and it varied notably. Fluctuations within a domain can be seen about a mean value

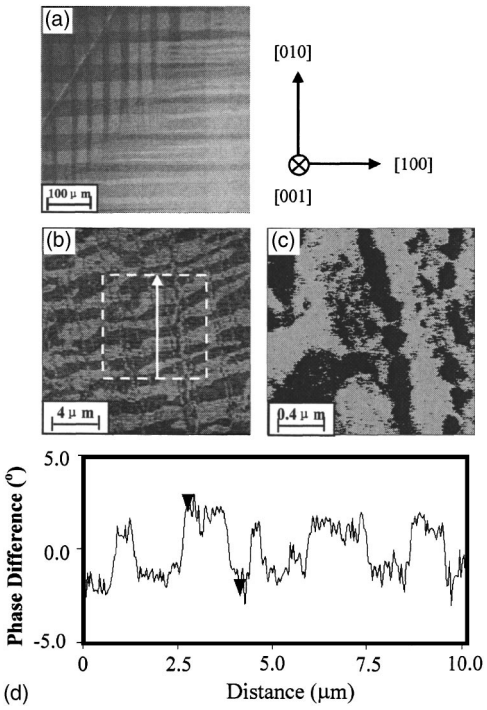

FIG. 6. Domain hierarchy of (001)-orientated PMN-40%PT in the ZFC condition, which is of the *T* phase. (a) Stripelike macrodomains with ⟨100⟩ preferred orientation by POM; (b) [100]-orientated striplike microdomains with fibrous subdomain structures by PFM; (c) high resolution PFM image illustrating irregularity; and (d) cross-sectional line analysis parallel to [010].

of the phase difference, possibly reflecting the local internal domain heterogeneities in Fig. 6(c) of this figure.

Figures 7(a) and 7(b) show POM and PFM images in the FC condition, respectively. The macrodomain plates in the PLM image can be seen to be similar to those for the ZFC condition in terms of size, an internal fibrous structure, and the presence of fringes. However, in the PFM image, comparisons of the internal fibrous structure between the ZFC and FC conditions will reveal that the {001} lamella domains

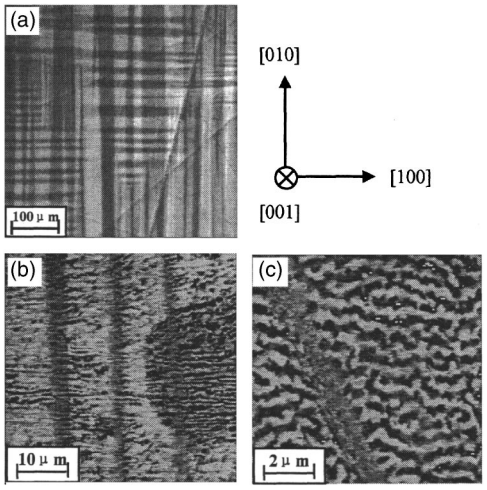

FIG. 7. Domain hierarchy of (001)-orientated PMN-40%PT in the FC condition, which is of the *T* phase. (a) Stripelike macrodomains with ⟨100⟩ preferred orientation by POM; (b) [100]-orientated striplike microdomains with fibrous subdomain structures by PFM; (c) high resolution PFM image illustrating irregularity; and (d) cross-sectional line analysis normal to [010].

are wider, longer, and more regularly spaced in the FC condition: application of E caused some to grow in a sidewise direction to the field and others to shrink. However, inspection of the lamella domains will reveal many internal irregularities, indicating that domain growth does not occur by a coherent boundary movement, but rather by the reorganization of internal irregularities.

IV. DISCUSSION AND SUMMARY

Our PFM results provide important insights into the nature of the domain-engineered state in PMN-x%PT crystals. The results demonstrate the presence of a domain hierarchy on various length scales, ranging from nanometers to millimeters, which depends upon the electrical history of the crystal. The findings can be summarized with respect to relevant phases.

For $x=20$ at. %, in phase X, the results show the presence of PND that do not self-assemble into macrodomain plates. The PND are essentially nonstress accommodating. The boundaries between them are not restricted by elastic compatibility. Field cooling aligns PND, however, it fails to induce the formation of normal micronsized domains or their assembly into macrodomain plates.

In phase R (i.e., the ZFC condition of PMN-30%PT), the PND assemble into wavy domains with some preferential orientation along {110}. These wavy domains then self-assemble into macrodomain plates that are oriented along {111}. However, in phase M_A (i.e., the FC condition of PMN-30%PT), the hierarchy of domain structures is notably changed, specifically resulting in a dramatic decrease in the domain size, although the macrodomain plates keep the same {110} orientation.

In phase M_C, for both the ZFC and FC conditions, the PNDs self-assemble into domain striations; however, there are important differences in the internal structure of the striations. The striations in the ZFC condition are long and preferentially oriented along only {110}; whereas those in the FC condition are more limited in spatial extent, consisting of zigzags between {010} variants about {110}. In both the ZFC and FC conditions, the domain striations self-assemble into much larger macrodomain plates which are oriented along {001}.

Phase T ($x=40\%$) consists of {001} oriented striations of micrometer size that have an internal nanoscale heterogeneity, which self-assemble into macrodomain plates of millimeter size oriented along a {001}. Application of E results in growth of some {001} striations at the expense of others, via reorganization of internal irregularities.

A. Origin of domain-engineering state

A natural question to ask is what is the origin of the domain hierarchy, and subsequent changes with composition and electrical history. It is important to compare our results with conventional ferroelectric "fingerprint" domains in $BaTiO_3$. In this case macrodomain plates have been observed, which contain internal fingerprint domains. Following conventional thought, these fingerprint patterns are 180° T domains whose distribution achieves polarization compensation; whereas the macrodomain plates are 90° ferroelastic domains, whose distribution achieves stress accommodation. Accordingly, in this classic case, a domain hierarchy exists, consisting of (i) micronsized 180° ferroelectric domains oriented along {001}, which exists inside of (ii) larger 90° ferroelastic domains, also oriented along {001}.

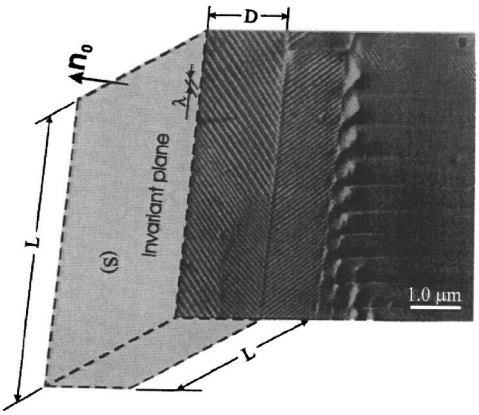

FIG. 8. Structure of a polydomain martensitic plate consisting of alternating lamellae of two twin-related orientation variants (domains) of the martensite shown by black and white. The boundary between the lamellae is the twin plane. The ratio of the "black" and "white" domain thicknesses provides the macroscopic invariancy of the habit plane. These plates fully fill a sample.[28]

So what is different in PMN-x%PT crystals? First, the fingerprints in PMN-x%PT crystals were oriented along {110} for both PMN-30%PT and PMN-35%PT. Second, the fingerprints were apparently built from finer scale polar structures or PND—there is an additional lower end of the hierarchal scale. Third, the *fingerprints* were quite irregular in morphology—the wavy domain boundaries indicate that random fields disrupt the long-range polar order, partially compensating the polarization. Thus, the domain hierarchy can not be completely adjusted at each length scale in an independent manner, i.e., polarization compensation and stress accommodation occur at all stages of the hierarchy, and not at separate length scales independent of the other. Fourth, fingerprints within macrodomain plates were found only in phases R, M_A, and M_C, and not in phases X and T. Finally, the fingerprints in PMN-x%PT crystals were very thin—the hierarchy consists of an extremely high domain wall density. In particular, the density of fingerprints was extreme near the MPB: at lower PT contents domain irregularities dominated the morphology and at higher PT contents fingerprints did not form.

1. Self-assembly due to stress accommodation in adaptive martensite

Alternatively, let us consider the conventional ferroelastic microstructure. On a fine length scale, alternating layers of twin-related domains exist, which also form a fingerprint pattern, as shown in Fig. 8.[28] The twin boundaries of the fingerprints are not restricted to be 180°. Self-assembly is achieved by varying the relative domain layer thicknesses of the fingerprints, which are adjusted to establish the macroscopic invariance of the habit plane,[29,30] and in doing so eliminating the long-range stress fields generated by crystal lattice misfits.[31–33] This requires the domain-averaged stress-

free transformation strain of each plate to be an invariant plane strain (IPS), where the invariant plane is parallel to the habit plane. Stress-accommodating alternating domain layers (or fingerprints) typical of ferroelastics will occur for any displacive transformation, which can form a domain-averaged transformation strain that is an IPS—including ferroelectrics.

On a longer length scale, minimization of the sum of the strain and interfacial energies drives a self-assembly of alternating domain layers into a polydomain plate, as also shown in Fig. 8. The typical domain size λ_o is related to the thickness of the polydomain plate D and the domain wall energy density γ as

$$\lambda_o = \beta \sqrt{\frac{\gamma}{\mu \varepsilon_o^2} D}, \tag{1}$$

where β is a dimensionless constant, μ is the shear modulus, and ε_o is the twinning strain.[23,24] It is a profound analogy that the typical thicknesses of ferroelectric and ferromagnetic domains in a plate of thickness D are also proportional to $\sqrt{\gamma D}$.

Recently, a theory for the conformal miniaturization of the self-assembled domain topology shown in Fig. 8 was developed.[34] This theory considered the case of abnormally small domain wall energy or extreme domain wall density. The theory was applied to ferroelastics and ferroelectrics containing miniaturized domains—in particular, to PMN-x%PT and PZN-x%PT crystals. It predicted the self-assembly of nanodomains into particular topologies, whose hierarchy was determined by stress accommodation and specific geometrical invariant conditions. The theory unambiguously predicted that the M phases of PMN-x%PT and PZN-x%PT are not homogeneous, but rather an adaptive mixed structural state with microdomain-averaged adjustable topological parameters. Changes in PND topology then resulted in changes in domain hierarchy, and also in an apparent phase stability.

2. Self-assembly of domain-engineered states in PMN-x%PT

In PMN-x%PT crystals, we believe three ingredients—stress accommodation, polarization compensation, and random fields—are key to understanding the domain hierarchy. Partial stress accommodation may occur at the fingerprint boundaries, in addition to partial polarization compensation. Also, hierarchal self-assembly is apparently complicated by random fields, which partially compensate the polarization.

At lower PT contents, random fields may limit self-organization of the domain hierarchy. Thus, only PND are observed, which do not assemble into striations or fingerprints, nor do macrodomain plates form. The domain morphology is nonstress accommodating. However, with increasing PT content, as the MPB is approached which has a significantly higher c/a ratio, stress accommodation of the PND may become critical. To minimize the elastic energy, the PND may begin to assemble into geometrical patterns that achieve the invariant conditions required of stress accommodation. Since the invariant plane for R and T domains lies along the {110} and {010}, it is natural that colonies of PND assemble with a morphology oriented along these two directions, as showed in Fig. 5(c). To achieve a more complete stress accommodation, macrodomain plates then form. At higher PT contents, in the T phase region, the domain hierarchy is much more like that expected of a conventional $C \rightarrow T$ phase transition in ferroelectric perovskites. Critical to the fine fingerprints is a low domain wall energy density—which is the key requirement for the conformal miniaturization of stress-accommodation. Our results show that this requirement is satisfied only in the vicinity of the MPB.

Field cooling may alter the distribution of PND. Thus, the domain hierarchy can be changed by electrical history. In the FC condition, for both PMN-30%PT and PMN-35%PT, the domain striations were reduced in size relative to the ZFC one. This significant increase in domain wall density may favor the conformally miniaturized stress-accommodating (or adaptive) ferroelectric state. In the ZFC condition, the lattice symmetry of PMN-30%PT is phase R, and x-ray reflections are relatively broad; whereas in the FC condition, the lattice symmetry is M_A, and the reflections considerably sharper.[20] Sharpening of the reflections also occurs in the M_c phase of PMN-35%PT on field cooling. Comparisons of these observations with the PFM images indicate that field cooling may favor a shorter-scale geometrical patterning of miniature polar domains. In this case, the reduction in the inhomogeneous line broadening may reflect a relaxation of the elastic strain energy between miniature domains, which also alters the domain hierarchy.

B. Summary

In summary, our results demonstrate the presence of a domain hierarchy on various length scales, ranging from nanometers to millimeters. Changes in the domain hierarchy with composition and electrical history of the crystal are discussed with respect to stress accommodation, polarization compensation, and random fields.

For $x=30$ at. % in the ZFC condition, phase R consists of PND that self-assemble into colonies close to a {110} which is spatially limited to <1 μm, which subsequently assemble into {111} macrodomain plates. However, in the FC condition, the domain size (of phase M_A) is dramatically decreased. For $x=35$ at. %, in both the ZFC and FC conditions, phase M_C consisted of PND that self-assembled into {110} striations, which subsequently self-assemble into {001} macrodomain plates. The {110} striations in the ZFC condition are long (tens of microns); whereas those in the FC condition are more limited in spatial extent (less than a micron).

ACKNOWLEDGMENTS

The authors gratefully acknowledge the support of the Office of Naval Research under Grant Nos. N000140210340 N000140210126, and MURI N000140110761.

[1] S.-E. Park and T. Shrout, J. Appl. Phys. **82**, 1804 (1997).
[2] B. Noheda, D. E. Cox, G. Shirane, J. A. Gonzalo, L. E. Cross, and S.-E. Park, Appl. Phys. Lett. **74**, 2059 (1999); B. Noeda, J. A. Gonzalo, L. E. Cross, R. Guo, S.-E. Park, D. E. Cox, and G. Shirane, Phys. Rev. B **61**, 8687 (2000).

[3]R. Guo, L. E. Cross, S.-E. Park, B. Noheda, D. E. Cox, and G. Shirane, Phys. Rev. Lett. **84**, 5423 (2000).
[4]D. E. Cox, B. Noheda, G. Shirane, Y. Uesu, K. Fujishiro, and Y. Yamada, Appl. Phys. Lett. **79**, 400 (2001).
[5]G. A. Smolenskii and A. Agranovskaya, Sov. Phys. Solid State **1**, 1429 (1960).
[6]L. E. Cross, Ferroelectrics **151**, 305 (1994).
[7]B. Noheda, D. E. Cox, G. Shirane, J. Gao, and Z. Ye, Phys. Rev. B **66**, 054104 (2002).
[8]J. M. Kiat, Y. Uesu, B. Dkhil, M. Matsuda, C. Malibert, and G. Calvarin, Phys. Rev. B **65**, 064106 (2002).
[9]G. Xu, D. Viehland, J. F. Li, P. M. Gehring, and G. Shirane, e-print cond-mat/0307144.
[10]P. M. Gehring, W. Chen, Z.-G. Ye, and G. Shirane, e-print cond-mat/0304289.
[11]C.-S. Tu, C.-L. Tsai, V. H. Schimidt, H. Luo, and Z. Yin, J. Appl. Phys. **89**, 7908 (2001).
[12]G. Xu, H. Luo, H. Xu, and Z. Yin, Phys. Rev. B **64**, 020102 (2001).
[13]Z.-G. Ye and M. Dong, J. Appl. Phys. **87**, 2312 (2000).
[14]D. Viehland, M.-C. Kim, Z. Xu, and J.-F. Li, Appl. Phys. Lett. **67**, 2471 (1995).
[15]Z. Xu, M. C. Kim, J.-F. Li, and D. Viehland, Philos. Mag. A **74**, 395 (1996).
[16]D. Viehland, L. E. Cross, J. Powers, and J. F. Li, Appl. Phys. Lett. **78**, 3508 (2001).
[17]D. Viehland, M. Wuttig, and L. E. Cross, J. Appl. Phys. **69**, 414 (1991).
[18]Y. Xi, C. Zhili, and L. E. Cross, J. Appl. Phys. **54**, 3399 (1983).
[19]Z. G. Ye, B. Noheda, M. Dong, D. Cox, and G. Shirane, Phys. Rev. B **64**, 184114 (2001).
[20]F. Bai, N. Wang, J. Li, D. Viehland, P. Gehring, G. Xu, and G. Shirane, J. Appl. Phys. **96**, 1620 (2004).
[21]M. Abplanalp, L. M. Eng, and P. Gunter, Appl. Phys. A: Mater. Sci. Process. **66**, S231 (1998).
[22]C. Hamagea, Ph.D. dissertation, Martin-Luther University, Halle-Wittenberg, Germany, 2001.
[23]C. Harnagea, A. Pignolet, M. Alexe, D. Hesse, and U. Gösele, Appl. Phys. A: Mater. Sci. Process. **70**, 261 (2000).
[24]M. Abplanalp, D. Barosova, J. Erhart, J. Fousek, P. Gunter, J. Nosek, and M. Sulc, J. Appl. Phys. **91**, 3797 (2002).
[25]I. K. Bdikin, V. V. Shvartsman, and A. L. Kholkin, Appl. Phys. Lett. **83**, 4232 (2003).
[26]W. Tan, Z. Xu, J. Shang, and P. Han, Appl. Phys. Lett. **76**, 3732 (2000).
[27]W. Zhu and P. Han, Appl. Phys. Lett. **75**, 3868 (1999).
[28]V. I. Syutkina and E. S. Jakovleva, Phys. Status Solidi **21**, 465 (1967).
[29]M. S. Wechsler, D. S. Lieberman, and T. A. Read, Trans. Metall. Soc. AIME 197, 1503 (1953).
[30]J. C. Bowles and J. K. Mackenzie, Acta Metall. **2**, 129 (1954).
[31]A. G. Khachaturyan and G. A. Shatalov, Zh. Eksp. Teor. Fiz. **56**, 1037 (1969) [Sov. Phys. JETP **29**, 557 (1969)].
[32]A. G. Khachaturyan, *The Theory of Structural Transformations in Solids* (Wiley, New York, 1983).
[33]A. L. Roytburd, Fiz. Tverd. Tela (Leningrad) **10**, 3619 (1968) [Sov. Phys. Solid State **10**, 2870 (1969)].
[34]Y. Jin, Y. Wang, A. G. Khachaturyan, J. F. Li, and D. Viehland, J. Appl. Phys. **94**, 3629 (2003).